Advanced Electronic Materials

ADVANCED ELECTRONIC MATERIALS Open Access

www.advelectronicmat.de

RESEARCH ARTICLE OPEN ACCESS

Enhanced Spin-Reorientation Transition and Polarization in $DyFeO_3$ Thin Films

Banani Biswas[1] | Bixin Yan[2] | Morgan Trassin[2] | Dirk Fuchs[3] | Ekatarina V. Pomjakushina[1] | Manfred Fiebig[2] | Thomas Lippert[1,4] | Christof W. Schneider[1]

[1]Paul Scherrer Institute, Aargau, Switzerland | [2]Department of Materials, ETH Zurich, Zurich, Switzerland | [3]Karlsruhe Institute of Technology, Institute for Quantum Materials and Technologies, Karlsruhe, Germany | [4]Department of Chemistry and Applied Biosciences, Laboratory of Inorganic Chemistry, ETH Zurich, Zurich, Switzerland

Correspondence: Christof W. Schneider (christof.schneider@psi.ch)

Received: 9 April 2026 | **Revised:** 25 June 2026 | **Accepted:** 28 July 2026

Keywords: $DyFeO_3$ | magnetic characterization | magnetism | orthoferrite | polar properties | thin films

ABSTRACT

Epitaxial strain in antiferromagnetic orthoferrite thin films is predicted to significantly enhance magnetic and polar properties with a shift of the polar response from below 4 K to room temperature and above by strengthening the rare earth-Fe interaction. In $DyFeO_3$, the Fe-spins undergo a spin reorientation transition between 40–50 K, and a magnetic field-induced ferroelectric phase transition is triggered by Dy ordering and displacement below 4 K. Here we report an increase in the spin reorientation temperature by more than 20 K in compressively strained $DyFeO_3$ films. The expected sharp spin transition is several 10 K wide, incomplete and largely suppressed, with the magnetic point group remaining at Γ_4 at all temperatures. The strain-induced Dy ordering above 4 K reduces the magnetic symmetry and introduces room-temperature polar order with the electrical polarization vector oriented along [100] and polarization values of more than 3 $\mu C/cm^2$.

1 | Introduction

Orthoferrites ($RFeO_3$) with a perovskite crystal structure (ABO_3) (Figure 1a) have been investigated extensively as bulk materials since the 1960s for their distinct magnetic ordering, involving high Néel temperatures ($T_N > 600$ K), canted antiferromagnetic (AFM) G-type spin structures with a spin reorientation transition (SRT) whose value depends strongly on the ionic size of the rare earth (R) element, and an AFM ordering of the R-ion at low temperatures (Figure 1b) [1–10]. At low temperatures, the magnetic properties of orthoferrites are therefore determined by the coexisting Fe and R-spin lattices with different AFM orders, giving rise to a frustrated interaction between the spins. The antiferromagnetically ordered Fe spins preserve the inversion symmetry of the ABO_3 crystal lattice, whereas a rare-earth spin ordering breaks it, thereby introducing polar order. The polar contribution is the result of a shift of the R-ion with respect to Fe as a means to lift the frustration. As a consequence, some but not all of the $RFeO_3$ compounds show ferroelectric (FE) properties [11], and the AFM ground state combined with the magnetically induced FE state gives rise to magneto-electric coupling.

Recently, this class of materials gained attention through studies of their low-temperature magnetic field properties [12] and the prediction that uniaxial stress will induce FE order even well above room temperature, potentially with a large electrical polarization [13, 14]. Such a room-temperature multiferroic state based on strain would have potential application in spin-based electronic devices.

Growth-induced strain is a well-studied and proven external parameter in thin-film growth to engineer physical material

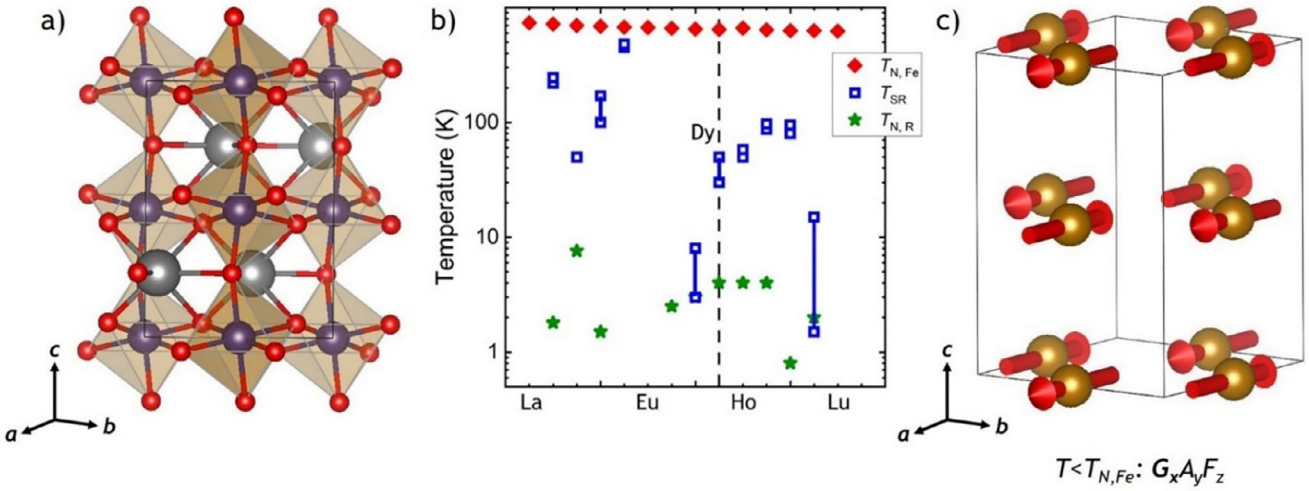

FIGURE 1 | (a) Crystal structure of $DyFeO_3$. (b) Temperature vs. *R* phase diagram displaying all known magnetic and polar transition temperatures for the different orthoferrites. (c) G-type AFM spin structure (Γ_4) for $DyFeO_3$ as derived from powder neutron diffraction measurements [31, 32]. Displayed is the Fe lattice.

properties by a defined change of lattice constants of the thin film system [15–18]. In thin films, strain can be introduced in two major ways. First, chemical pressure, in which an atom is replaced by another atom [19–21]. Second, by epitaxial strain, in which the lattice mismatch between substrate and film determines the amount of strain [22–26]. As the lattice parameters influence the bond length and angle by changing the relative positions of atoms in a unit cell, the electronic distribution and their interaction can change. Hence, strain has the means to alter the mechanical, chemical, electrical, and magnetic properties of a material [27].

$DyFeO_3$ is a special member of the $RFeO_3$ family known to have magnetic ordering-driven multiferroic properties below 4 K with magneto-electric coupling [4, 6, 28]. It has a distorted perovskite crystal structure with a three-dimensional array of corner-sharing metal-oxygen octahedra (DyO_6 and FeO_6), and tilted Fe-O octahedra along the [001] direction (Figure 1a). The interaction between the two cations causes three different exchange interactions, namely Fe^{3+}–Fe^{3+}, Dy^{3+}–Fe^{3+}, and Dy^{3+}–Dy^{3+}, which dominate at different temperature regimes. The strong Fe^{3+}–Fe^{3+} interaction causes the ordering of the Fe lattice at $T_{N,Fe}$ = 645 K with a G-type AFM ordering along the *a*-axis, which preserves the inversion symmetry of the crystal lattice (Figure 1c). Due to the Dzyaloshinskii-Moriya (DM) interaction, a tilting of the oxygen octahedra gives rise to a weak ferromagnetic (wFM) component along [001] and A-type AFM ordering along [010]. This spin state is known as Γ_4 and represented as $\mathbf{G}_x\mathrm{A}_y\mathrm{F}_z$ in Bertaut's notation [29].

The strength of the interaction between Dy and Fe (Dy^{3+}–Fe^{3+}) increases with decreasing temperature, leading to a spin reorientation (SR) of the Morin type, a first order spin transition, with a spin reorientation temperature T_{SR} between 40–60 K. This is the consequence of Fe-spins switching from the *a*- to the *b*-direction, and the wFM component along [001] disappears [4–6, 12, 30] with the spin state changing from Γ_4 to Γ_1 ($A_x\boldsymbol{G}_yC_z$). At around 4 K Dy orders antiferromagnetically ($T_{N,Dy}$) with the Dy-spins aligned in the *ab* plane ($G_x\boldsymbol{A}_y$) [6]. Rare-earth ordering would break the inversion symmetry, since the coexistence of the two competing AFM orders is realized by a frustrated interaction between Fe and *R* spins, forming two interpenetrating cubic sublattices. The Dy-ordering is assumed to be commensurate, but recent neutron powder experiments show an incommensurate Dy ordering [31–33]. An incommensurate state would compensate the frustration of the two spin lattices and hence explain the absence of polar order below $T_{N,Dy}$.

Polar order is restored by applying a magnetic field larger than ~2.3 T along [001] thereby displacing Dy. As a result, the Γ_1 phase switches back to the more stable Γ_4 phase [4]. Interestingly, uniaxial pressure applied along [110] also introduces a FE polarization with the FM moment parallel to [001] as a result of reducing the magnetic point group symmetry from 222 to 2 [34]. With a modest pressure of 1.51 kbar (151 MPa) and no magnetic field applied ($H = 0$), an electrical polarization of 4.5 nC/cm^2 at 2 K has been measured [34]. Unlike magnetic field-induced FE order, this pressure-induced polar state vanishes at $T_{N,Dy}$. There is also a report where a switchable electric polarization above T_{SR} has been observed along [100] when poling was carried out across the SRT while cooling and measured while warming. This indicates that magnetic ordering of the *R* ions is not a necessary condition to induce FE; a dipolar displaced *R* ion in the Γ_4-phase (wFM) is sufficient [8, 35]. A further characteristic of orthoferrites is an induced magnetic moment *M* from the Fe spin lattice into the rare-earth sublattice below $T_{N,Fe}$ when applying a magnetic field along [001]. This has been theoretically shown for $GdFeO_3$ [36], but it applies to all orthoferrites [2, 37].

In this work, we show the effect of strain on the magnetic and polar properties of multiferroic $DyFeO_3$ grown as thin films with different thicknesses on (010)-oriented $YAlO_3$ substrates. X-ray diffraction verifies compressive in-plane strain for the [100] and [001] direction giving rise to complex orientation-dependent magnetic thin-film properties. These magnetic

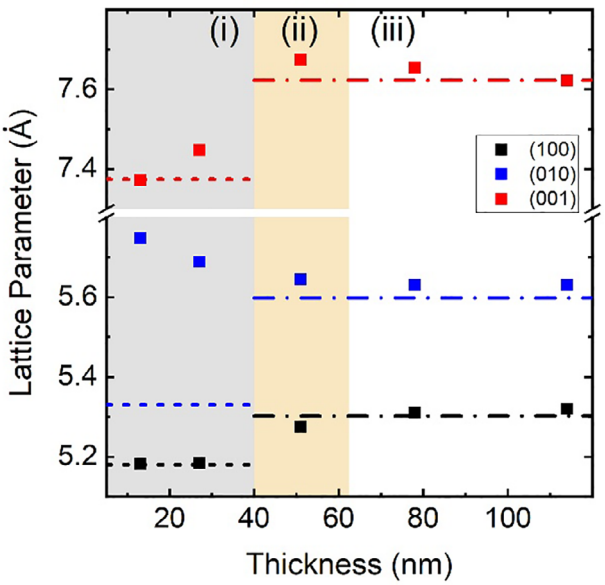

FIGURE 2 | Lattice parameters vs. film thickness for the three main axes of $DyFeO_3$ films. Marked as horizontal dashed-dotted lines are the bulk values for the $YAlO_3$ substrate and $DyFeO_3$.

properties can be derived and explained from temperature-dependent single-crystal measurements of the magnetic moment along the three main crystalline orientations. This is complemented by temperature-dependent magnetic measurements of strained (010)-$LuFeO_3$ thin films comprising only one active spin lattice. Strain increases T_{SR} by more than 20 K and is very magnetic field sensitive. To demonstrate polar properties, temperature-dependent electrical polarization measurements are shown, giving rise to a FE response up to 260 K with $P \| a$ and polarization values of 3 μC/cm^2, whereas for bulk the ferroelectric phase appears below 4 K only in the presence of a magnetic field along the *c*-axis, ***P*** parallel [001] and with polarization values of the order nC/cm^2. Measuring films with different strain also allows mapping ferroic single crystal properties onto a tentative temperature vs strain phase diagram.

2 | Results and Discussion

2.1 | Structural Characterization

All (010)-oriented films investigated were grown by pulsed laser deposition (PLD) with a thickness-dependent tensile strain for the out-of-plane direction due to a shortening of the in-plane lattice constant induced by the substrate epitaxial strain [38]. For films of around 10 nm, it is of the order 2–3% and decreases to <1% for films with a thickness of 100 nm or more. Films with a thickness between 15 – 20 nm grow coherent with the in-plane axes align macroscopically with the substrate [38]. The full-width-half-maximum of the *in-plane* film rocking curve is as narrow as the substrate and instrumentally resolution limited (< 0.003°) [38]. Thicker films show a relaxation towards the bulk $DyFeO_3$ Bragg position, but some remnants of the initial coherent layer can still be found. Evaluating the lattice parameters for the different films we can distinguish three regimes with a change-over in the 40 nm range film thickness (Figure 2). For films thinner than 40 nm (region (i)), they are highly strained with a constant unit cell volume of ~219 Å^3 and no measurable relaxation towards $DyFeO_3$ bulk. Whereas films thicker than 40 nm are partially strained or almost relaxed (region (ii), (iii) [38]) and the constant unit cell volume (~229 Å^3) is similar to that of unstrained $DyFeO_3$ (~226 Å^3). This is also reflected when calculating the out-of-plane strain, which is for the 13 nm and 27 nm film ~2.6% and ~1.6%, respectively, and ~0.6% for films thicker than 40 nm. Strain values for the $DyFeO_3$ films discussed are listed in Table 1. The quality of these films was also checked using μRaman. Except for the $B_{2g}(6)$ at 534 cm^{-1}, a O(2)-Fe-O(2) scissor-like bending mode, no other mode can be resolved due to the strong substrate contribution. However, the $B_{2g}(7)$ at 612 cm^{-1}, often overlapping with an oxygen vacancy Raman mode at ~620 cm^{-1}, is very small and consistent with the $DyFeO_3$ Fe-O(2) stretching mode. For comparison, the Raman spectrum for the single crystal shows all Raman modes at the expected energies, including the absence of the vacancy mode at ~620 cm^{-1} (see SI 2) [39, 40].

2.2 | Magnetic Properties

2.2.1 | $DyFeO_3$ Single Crystal

Let us first start with a reference single crystal; the temperature-dependent magnetic measurements ($M(T)$) between 2 and 300 K are shown in Figure 3a, inset. We observe two magnetic transitions, one at ~6 K and one at ~41 K, with the first one being $T_{N,Dy}$, the latter T_{SR} (Figure 3a, inset) [31]. The expected AFM transition for Fe $T_{N,Fe}$ ~645 K cannot be measured due to instrumental limitations (see Methods section). Above 6 K, the magnetization along [100] and [010] decreases, while along [001] it increases until, at 41 K, a sharp rise in the magnetization is observed, signaling the Fe spin-flip from the *b*- to the *a*-direction as determined from neutron diffraction measurements [31]. Above T_{SR}, the canting of the Fe-O octahedra gives rise to a small FM contribution (wFM) along the *c*-direction, an F_z component consistent with Γ_4. Below T_{SR} the spin state is described by Γ_1 since the FM contribution is absent. The moment reaches ~0.15 μ_B/f.u. at T_{SR} using a 0.1 T probing field (μ_B: Bohr magneton; f.u.: formula unit) for the *c*-direction whereas in the [100] and [010] directions it is up to 80% smaller (see Table 1). Measuring $M(H)$-loops up to 4 T along [001], the moment remains at 0.15 μ_B/f.u., which indicates a FM alignment of Dy spins to compensate the AFM moment from the Fe spin lattice.

2.2.2 | $DyFeO_3$ Thin Films

Moving on to the thin films, we begin with the 115 nm film, which has the most relaxed structure and $M(T)$ is expected to be similar to single-crystal data. Like for the single-crystal (Figure 3a, inset), two ordering temperatures are noted: A Dy ordering at ~4.5 K for the *a*- and *b*-direction, and above $T_{N,Dy}$ a change in moment along [001] spanning several 10 K. This change in moment is associated with the spin reorientation transition starting at ~70 K with a maximum change of moment of ~20% towards lower temperatures whereas for the single crystal the initial drop in moment is ~95%. For the [100] and [010] directions, there is no noticeable signature of T_{SR} at ~70 K. However, along [001], a

TABLE 1 | Values of the lattice mismatch, ordering temperatures, and magnetic moments for a $DyFeO_3$ single crystal and $DyFeO_3$ thin films with different strains.

	Strain (%)	T_{SR} [K] @ 0.01 T	$T_{N,Dy}$ [K]	$M@T_{SR}$ [μ_B/f.u.]
DFO	**SC**			
[100]	—	—	~4	0.06@0.1T
[010]	—	—	~4	0.03@0.1T
[001]	—	41	—	0.15@0.1T
115nm	**DFO**			
[100]	0.33	56.8	~4.5	~0.95@0.1T
[010]	0.6	44.9	~6	~1.55@0.1T
[001]	0	58.3	< 3	~0.8@0.1T
13nm	**DFO**			
[100]	−2.22	86.7	~4.5	~2.4@0.1T
[010]	2.5	33.6	~4.5	~2.0@0.1T
[001]	−3.46	91.8	< 3	~5.3@0.1T
12.2nm	**LFO**			
[100]	−0.73	—	—	—
[010]	−4.23	—	—	—
[001]	−2.71	—	—	—

low-temperature $M(T)$ upturn starts at ~17 K, leading to a Dy ordering below 3 K. $DyFeO_3$ films therefore order antiferromagnetically along all three crystallographic directions, whereas Dy-ordering for a single crystal takes place in the *ab*-plane. In Table 1, the measured moments at T_{SR} are summarized and turn out to be larger than reported for a single crystal [31]. At $T_{SR,}$ the spin transition along the *c*-axis is rather broad and occurs over more than 40 K, unlike the abrupt drop in moment for the single crystal (Figure 3a, inset). One way to establish a value for T_{SR} for the [001] direction is to calculate the derivative dM/dT and measure the intersection of the two linear slopes one can place on dM/dT, as exemplarily shown in Figure S5. The extracted value for T_{SR} = 66.2 K for H = 0.1 T. To determine the spin propagation vector above and below T_{SR} for films neutron diffraction measurements analogous to single-crystal measurements are required [31]. This is at present not possible for these very thin films due to a lack of sample volume and insufficient scattering properties. Assuming the direct analogy to a single crystal, the Fe-spin will be pointing along [100] above T_{SR} and along [010] below.

Orientation-dependent $M(T)$ measurements for the highly strained 13 nm film show one clear ordering temperature, $T_{N,Dy}$ ~4.5 K for the *a*- and *b*-directions, and potentially T_{SR} 54.8 K for Fe along the *b*-direction (Figure 3b). T_{SR} for the *c*-direction is at 77.5 K and drops very slowly with decreasing temperature until at the minimum at ~12 K, the moment rises again towards lower temperatures. For the 115 nm film, this is taken as evidence of an increase in Dy^{3+}-Dy^{3+} interactions leading to antiferromagnetic Dy ordering in the *ab*-plane below 4.5 K. It is interesting to note that T_{SR} is strain and magnetic field dependent. The value of 54.8 K measured at 100 mT for the *b*-direction is similar to values reported for single crystals, albeit the applied field of 100 mT pushes T_{SR} down to 8 K for a single crystal. For a typical field of 10 mT to determine T_{SR}, the value for the *b*-axis of the highly strained film is still 54.8 K and therefore unchanged. Compressive strain, however, results in larger values for T_{SR} analogous to pressure-dependent neutron diffraction measurements on single crystals [31]. This suggests that strain and magnetic field are strong tuning parameters to change physical properties of thin films.

The apparent anisotropy in T_{SR} as noted in Table 1 is not plausible for films if the spin direction changes from [001] to [010], as in a single crystal. Reanalyzing $M(T)$ for the single crystal along all three crystallographic directions by calculating dM/dT, the onset of the steep drop at around 43 K along the [001] direction marks the start of the spin reorientation as verified by neutron scattering [31]. The onset of the foot structure around 38 K coincides with signatures in the derivative for the [010] direction, and the start of the spin reorientation at around 43 K can also be identified for [100]. Applying this finding to thin-film data, the numbers extracted for T_{SR} along [001] and [100] indeed represent the onset of T_{SR}, whereas the temperature values along [010] represent the lowest point reached, where spins turn from [100] to [010]. If the SRT is fully completed, like in a single crystal, meaning all spins flip from [100] to [010], then a drop of 5% of the magnetic signal for a film corresponds to 5% of all Fe-spin pointing along [100] flipped to the [010] direction.

Applying a magnetic field changes the Dy^{3+}-Fe^{3+} interaction and as a consequence $M(T)$. This is shown in (Figure 3c) where $M(T)$ for the 13 nm film has been measured with probing fields of 10 and 100 mT for the [100] and [001] directions. The influence of the applied fields for both directions is:

i. a sign-change of the $M(T)$ slopes at temperatures above ~100 K;

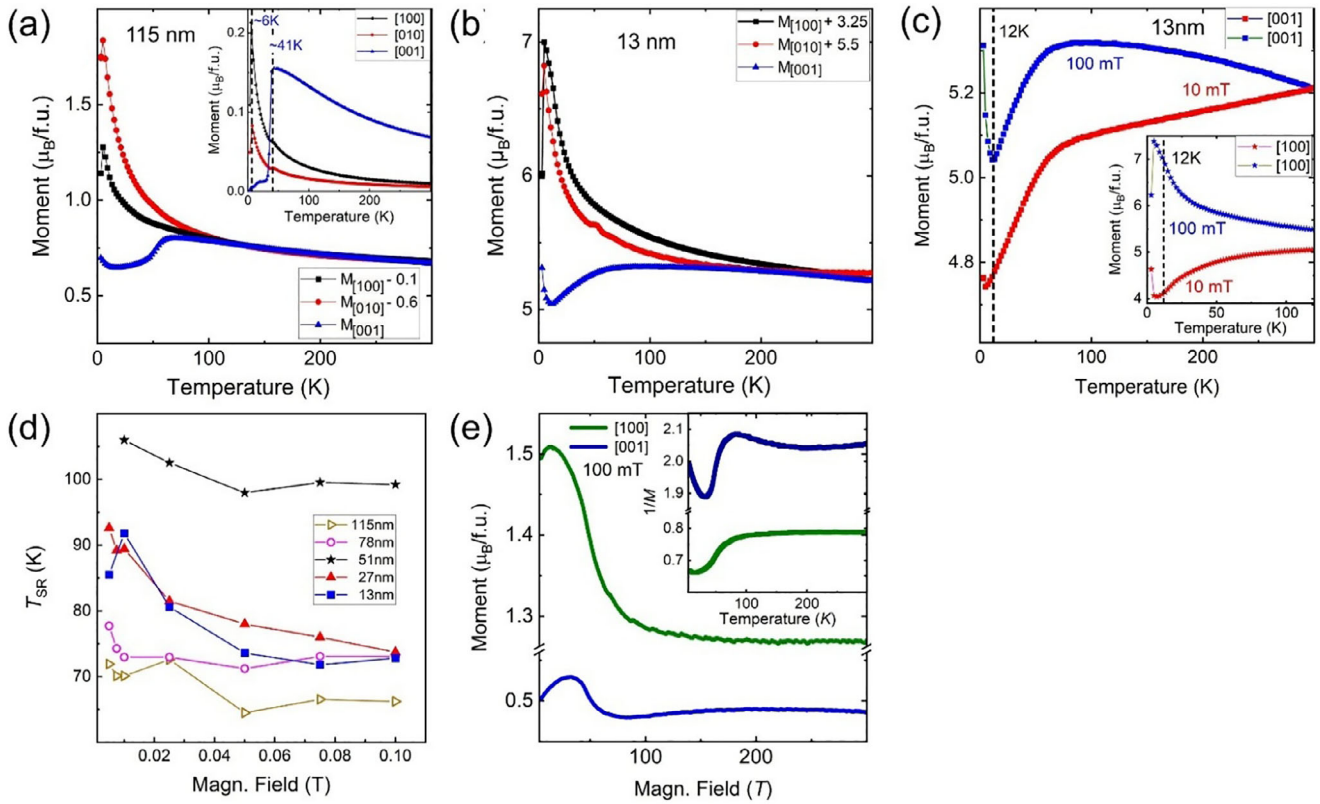

FIGURE 3 | (a) Zero field cooled (ZFC) $M(T)$ measurements of a 115 nm, [010]-oriented $DyFeO_3$ thin film along [100], [010] and [001] with a magnetic field of $H = 0.1$ T. Data for [001] are taken from [41]. The axis has been scaled along [100] and [010] to fit all three measurements in one figure; inset: ZFC measurements of the $DyFeO_3$ single crystal. Data from [31]. (b) ZFC measurements of a 13 nm, [010]-oriented $DyFeO_3$ thin film along [100], [010], and [001] with a magnetic field of $H = 0.1$ T. Data for [001] are taken from [41] and measurements for [010] and [001] have been rescaled along [100] and [010] to fit all three measurements in one figure. (c) ZFC measurements of a 13 nm, [010]-oriented $DyFeO_3$ thin film along [001] with a magnetic field of 0.01 and 0.1 T. Data for [001] at 100 mT are taken from [41]. Inset: magnified temperature window for [100] between 3 and 120 K. (d) Spin reorientation temperature vs. applied magnetic field along [001] for films of different thicknesses. T_{SR} has been determined from the intersection point between the onset and steep slope of dM/dT. The corresponding data are shown in [42] on p. 120. (e) ZFC measurements of a 12.2 nm, [010]-oriented $LuFeO_3$ thin film along [100] and [001] with a magnetic field of $H = 0.1$ T. Inset: $1/M(T)$ for the 12.2 nm $LuFeO_3$ film along [100] and [001].

ii. slopes are in parts strictly linear [45].

In addition, a magnetic field sensitive broad transition starts around 77.5 K with a minimum at 12 K for the [001] direction measured with 10 mT and 5 K with 100 mT. A similar minimum at 5 K is measured for the [100] direction with a field of 10 mT, whereas with 100 mT it is a drop at ~4 K, the temperature where Dy ordering sets in. These significant changes in $M(T)$ are related to Fe-spins, which induce a magnetic moment at the Dy site [43–45]. This is equivalent to known bulk properties [36]. For small fields, the Dy alignment is antiparallel, which will change to a parallel spin configuration for larger fields [41]. As soon as a magnetic field is applied, a polar component is introduced and hence an electric dipole moment will be active.

The small applied probing fields for ZFC measurements affect T_{SR}. For a single crystal, T_{SR} will be suppressed [12, 31], for films, the outcome is shown in Figure 3d for compressive strain along [001]. Values for T_{SR} are strain and field-dependent and range between 60 and 105 K as measured at 5 mT. For fields between 5 and 100 mT, T_{SR} is reduced by more than 10 K for all films. This is less than reported for single crystals (>30 K) [12, 31]. The systematic suppression of T_{SR} with increasing magnetic field is therefore analogous to known single crystal properties, but strain-related properties (increase in T_{SR}) are convoluted with magnetic field-dependent properties (decrease in T_{SR}), and the overall net effect in the field-induced reduction of T_{SR} is smaller than expected. All $M(T,H)$ data measured along [001] for films with different thicknesses are shown in Figure S6.

With decreasing temperature, the Dy-Fe interaction in $DyFeO_3$ forces the spin direction from the *a*- to the *b*-direction. For a single crystal, the change in the spin direction is close to 100%, for the strained films the total change in moment below T_{SR} can be as small as ≈5%. The observed changes in $M(T)$ for $DyFeO_3$ films can be the result of the distorted Fe-spin lattice. Measuring $M(T)$ for a 12.2 nm thick [010]-oriented $LuFeO_3$ thin film along [100] and [001], both temperature dependencies do not follow the expected Curie-Weiss dependence (Figure 3e) but show temperature-dependent broad features similar to $M(T)$-measurements of the two-spin system $DyFeO_3$. This is highlighted when plotting $1/M(T)$ for both directions (Figure 3e, inset). These measurements demonstrate that the Fe-spin lattice is very susceptible to compressive strain. For $DyFeO_3$ thin films, this means a competition between strain and Dy^{3+}-Fe^{3+} interaction with opposite sign for

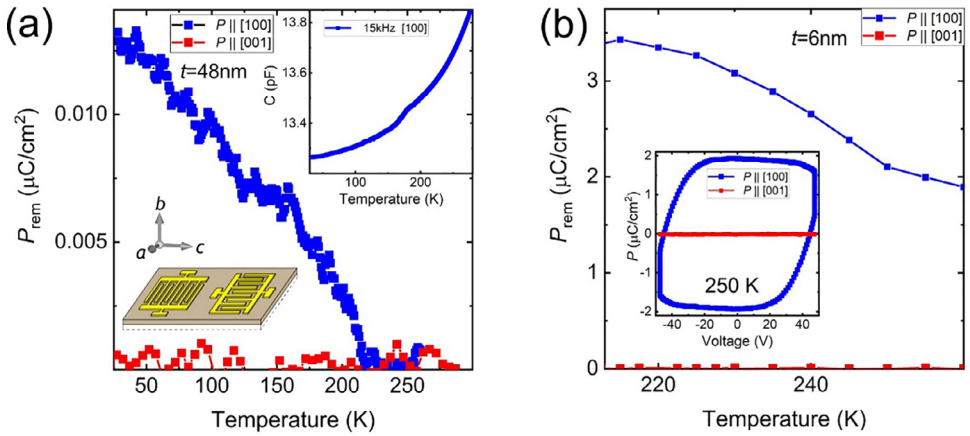

FIGURE 4 | (a) Remanent polarization vs. T of a 48 nm $DyFeO_3$ film along [100] (blue) and [001] (red). Inset: Capacity vs. T along [100]. Schematic of the alignment of the interdigitated measurement structure. (b) Remanent polarization vs. T of a 6 nm $DyFeO_3$ film along [100] and [001]. Inset: $P(V)$ along [100] and [001] measured at 250 K.

the moment, leading to a significant increase in the transition width of $M(T)$ below 100 K.

If a displacement of the Dy atoms in the unit cell plays a role in a manner equivalent to the bulk when applying a magnetic field below $T_{N,Dy}$ is unknown [4, 6]. The displacement of Dy in a single crystal below $T_{N,Dy}$ is the result of the Fe^{3+}-Dy^{3+} exchange interaction. It induces a displacement of the Dy^{3+} ions towards the Fe^{3+} ions with opposite spin to minimise the (AFM) exchange energy. For the single crystal, a magnetic field of ~2.3 T is required to change from an incommensurate Dy ordering to a commensurate state [33] and to overcome the exchange energy in order to displace Dy along [001], while for films the Dy influence is found to be dominant along [001] and [100]. In addition, the coercive field between room temperature and 3 K is close to 1 T [38]. The magnetic influence of Dy in two crystallographic directions is already a violation of the magnetic symmetry and should therefore lead to a polar state.

2.3 | Polar Properties

Motivated by the experimental finding of two distinguished orientations with respect to magnetic properties, which is also mirrored by double steps in magnetic hysteresis loops [38] where the orientation dependence of H_{C2} is suggestive of [100] being the likely polar axis instead of [001] as reported for single crystals, we probed the potential FE behaviour of a 48nm thick film along [100] and [001] with two independent orthogonal interdigitated structures to experimentally determine the direction of a polar axis [46–48]. The interdigitated structure has an aspect ratio of more than 400 between the long and short axes to ensure that the measurement predominantly detects the signal for the selected in-plane directions, not for the orthogonal direction. Interdigitated structures consisting of 361 fingers separated by a gap of 5 μm were patterned to measure the capacity and electrical polarization ($P(E)$) loops between 50 K and 300 K (Figure 4a). The onset of a remanent polarization was measured at ~220 K for the [100] direction, and no measurable signal was detected above the noise level along [001]. With decreasing temperature, P_{rem} reached a small plateau at ~162 K and started to rise again at ~125 K, reaching a value of 0.014 μC/cm² at 50 K. This kind of temperature dependence would suggest not a single order parameter but the presence of two. We measured in addition $C(T)$ for the [100] direction and observed a frequency-independent signature starting at ~190 K (see inset Figure 4a). This signature is indicative of a polar response and does not correspond to the plateau region of the order parameter. Since the measured polarization is small and the signature for $C(T)$ not pronounced, it is expected that the onset of the capacity change is lower than the onset of P_{rem}. The likely reason is a strain- related relaxation in the film and the introduction of defects, as observed for these films in reciprocal k-space maps.

Low polarization values were often recorded for thicker films along [100] (> 30 nm) and no response along [001]. The $DyFeO_3$ films typically suffered from leakage currents at temperatures around room temperature and above, whereas at low temperatures, the resistance of these layers exceeded the input impedance of the LCZ meter. Leakage currents for PE-loop measurements are accounted for using the positive-up negative-down (PUND) measurement scheme. One measurement of a highly insulating film is shown in Figure 4b where $P_{rem}(T)$ of a 6 nm thin layer has been measured. A polar response is recorded along [100], none along [001]. These measurements for the two orthogonal in-plane directions, where a polar response is expected, prove two points: First, these films are twin-free as shown by reciprocal space mapping. Second, charging cannot be the primary reason for the incomplete PE-loops since this would result in an isotropic response. Still, leakage currents are affecting PE-loop measurements, with an intrinsic mechanism being the origin for these currents. One potential explanation is a double exchange interaction between spins giving rise to conducting electrons, which can result in large magnetic moments (see Figure 2). Alternatively, an orbital magnetization contributes to the total moment.

For a 6 nm film, polarization values larger than 1μC/cm² below 260 K have been measured, reaching a maximum of 3.2 μC/cm² at 215 K before starting to decrease as a consequence of a too small applied electric field to fully align the electric dipole moments at lower temperatures (Figure 4b). The leaky films

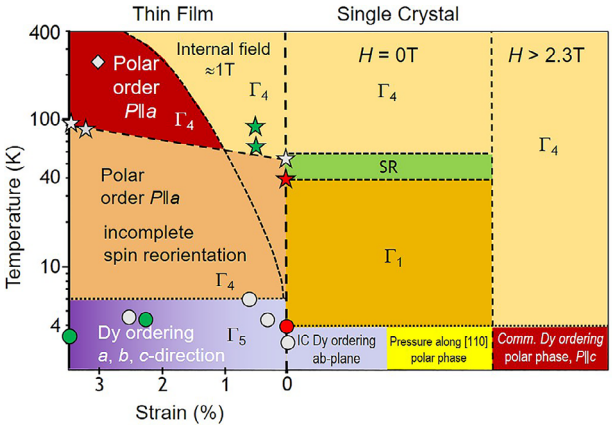

FIGURE 5 | Tentative compressive strain vs. T phase diagram for $DyFeO_3$ films indicating the different magnetic and polar phases. This is compared to single crystal magnetic and polar properties. The single crystal phase diagram is based on literature data [1, 4, 11, 12, 31–34, 38, 51]; the thin film part is our own data [31, 38, 41, 42]. For T_{SR}, data taken at 0.01T are shown for the [001]-direction; green represents tensile strain, grey represents compressive strain, and red represents single crystal data. Circle: $T_{N,Dy}$; Star: T_{SR}; Diamond: T_{FE}.

prevented conclusive measurements at room temperature and above, but signatures of a polar response for the [100] and none for [001] on the same film have been observed up to 390 K. The observation of a polar response is in line with room-temperature PFM measurements showing room-temperature polar switching for $YFeO_3$ and $LuFeO_3$ thin films [49, 50]. The direction of P, however, was reported along [001] which is in contradiction to the presented measurements of coherent, strained thin films and theoretical expectations [13, 14]. We also note that measurements at room temperature and above with the interdigitated structure have shown a polar response along [100] albeit superimposed by leakage, and no response along [001] with very little or no leakage. This general observation is consistent with a polar state and not simple charging, where an isotropic response is expected.

Second harmonic measurements have been conducted at room temperature in reflection and transmission for the 13 nm $DyFeO_3$ film with P pointing along [100]. These measurements are in line with expectations but not conclusive (see Figure S3).

2.4 | Discussion

From the presented magnetic and polar data for coherent (010)-oriented $DyFeO_3$ thin films with anisotropic, compressive strain, it is clear that ferroic film properties show up very different to bulk properties but can be traced back to known single crystal characteristics. This is most noticeable for the spin reorientation, where the clear signature of the SR as reported for a single crystal is missing and at temperatures below 10 K, a Dy ordering can be observed for all three main crystallographic axes, an ordering temperature which is larger than bulk $T_{N,Dy}$. The correlation between compressively strained film vs. single crystal properties is visualized in Figure 5 as a tentative strain phase diagram and will be discussed in the following. Boundaries are taken or deduced from literature and own work and are often not strictly known [1, 4, 11, 12, 31–34, 38, 41, 42, 51]. In particular, for the polar film boundary, intrinsic material issues prevented a further detailed study to deduce a more conclusive borderline.

2.4.1 | Effect of Compressive Strain on T_{SR}

The compressive in-plane lattice strain increases T_{SR} and the amount of epitaxial strain corresponds roughly to the compressive strain utilized in uniaxial pressure experiments on $DyFeO_3$ single crystals. For a $DyFeO_3$ single crystal T_{SR} increases with 2 K/kbar (not shown in Figure 5) [38]. Comparing the observed values of T_{SR} with the changes in lattice parameters, a rise of T_{SR} between +20K and +40K can be expected based on the lattice mismatch. An increase by ≈30 K for the different crystalline directions therefore fits well to the expected temperature range.

2.4.2 | Spin Reorientation Transition

For single crystals, we have shown that compressive strain increases T_{SR} but the transition width of the SR remains unaffected [38]. Unlike with an applied magnetic field [31]. It suppresses and moves T_{SR} to lower temperatures, thereby partially blocking the spin flip. Depending on the direction of the applied field, this leads to a broadening of the SRT, and the measured magnetic signal along [001] never goes to zero with decreasing temperature. In addition, with increasing magnetic field, $T_{N,Dy}$ shifts to higher temperatures and suppresses the spin-flip at lower temperatures [31].

It is interesting to note that the typically sharp SRT for $DyFeO_3$ is a first-order spin transition. For single crystals, the SRT is completed within a couple of Kelvin, whereas for strained films the nominal transition width can span several 10 K, often showing a more complex field-dependent structure and still be incomplete. For single crystals, the point with the largest curvature dM/dT can be used as a criterion to determine T_{SR}. This criterion will not work for thin films the same way, and the intersection point between the onset and the steep slope of dM/dT is a good approximation. The reason is the strain-enhanced Fe-Dy interaction strength showing its influence already at temperatures well above T_{SR} as a continuous change in curvature for $M(H)_{[001]}$, which looks like a very large shift of T_{SR} to higher temperatures. For single crystals, similar but smaller changes for $M(H)$ along [001] are measured, but neutron measurements clearly show that T_{SR} is directly correlated to the step in $M(H)$.

2.4.3 | Spin Flip Suppression

Based on the discussion about T_{SR}, anisotropic compressive strain in coherent films will therefore have at least two consequences. First, the shortening of the bonds leads to a strengthened Dy-Fe interaction and changed magnetic properties as compared to a single crystal. Second, the Fe-spin lattice is very susceptible to strain, and the typical signatures for T_{SR} are washed out and depend on the strength of the applied probing field (see Figure 3c,d). The expected outcome on $M(T)$ would be a significant shift of T_{SR} to higher temperatures (compressive strain), a

broadening of SRT due to the strained Fe lattice, and with the stronger Fe-Dy coupling an enhanced magnetic field sensitivity. The strain effects on the Fe lattice and magnetic field sensitivity are therefore the most likely reason for the very extended and incomplete transition below T_{SR}. In addition, there are large intrinsic magnetic fields along [001] and [100], which will affect T_{SR}. Expected is a strong suppression of $T_{SR,}$ but this seems not to be the case irrespective of tensile or compressive strain. Remarkable is the finding that films with small strain values fall into the expected temperature window where T_{SR} is measured for single crystals (between 40 K and 60 K), whereas the more strained films show much higher values.

The very broad and incomplete transition measured for the strained films is suggestive of a continuous change in the spin direction, which can be associated with a second-order transition. A transition from a first-order to a second-order is possible but requires a broken symmetry or a critical point. Alternatively, the transition from Γ_4 to Γ_1 does not take place in films down to the lowest temperature measured because the spin-flip is blocked either by the strained Fe-lattice or the large internal magnetic fields existing along [100] and [001] [52]. Consequently, the magnetic symmetry for films remains $\mathbf{G}_x\mathrm{A}_y\mathrm{F}_z$ throughout the entire temperature window between $T_{N,Dy}$ and room temperature and above. This scenario of a Γ_4 phase is consistent with the observation of an exchange bias below T_{SR} as reported in [38].

A uniaxial pressure along the [110]-direction of the $DyFeO_3$ unit cell reduces the magnetic point group symmetry 222 to 2 [34], and as a consequence, a FE polarization is introduced with P parallel [001] for $T < T_{N,Dy}$. The highly distorted film unit cells indicate a symmetry group different from unstrained $DyFeO_3$ [13, 14, 34]. As a result, the Γ_4 phase exists between 1.8 K and 390 K with a wFM contribution for [100] and [001] and an observable exchange bias below T_{SR}. Likewise, the introduction of strain results in a magnetic anisotropy giving rise to double-step hysteresis loops along [100] and [001] [38, 41], indicating that the [100] direction should be the preferred direction for the electrical polarization [38]. This would be in agreement with the orientation-dependent $P(E)$ and opical second harmonic generation (SHG) measurements (see SI [40]).

2.4.4 | Polar Properties

With Dy forming a magnetic field-induced second spin lattice, it is reasonable to assume that the magnetic symmetry of this spin lattice is low and hence provides a possible explanation of a polar response at temperatures well above $T_{N,Dy}$. For the single crystal, a field of ∼2.3 T is required to break the incommensurability and drive $DyFeO_3$ polar by displacing Dy along [001]. For the strained films the internal field of Dy is ∼1 T [38]. We therefore have the scenario of a magnetic anisotropy-driven FE giving rise to a magnetic response of the rare-earth element, whereas for the single crystal, it is a magnetic field induced polar response which ends at $T_{N,Dy}$. However, the electric measurements for films above $T_{N,Dy}$ were done without an applied magnetic field. The interpretation, therefore, is an electric field-induced polar state and thus indirectly proves magneto-electric coupling, albeit the state seems not to be very stable if the applied fields are too small [33, 38]. From the presented experiments, it is not possible to deduce the origin of the polar response. A possible explanation is displaced Dy. However, if film and bulk behave similarly, then a polar response should vanish above $T_{N,Dy}$. Alternatively, it is theoretically predicted that compressively strained films can take on a P4mm, a $P2_{1am}(I)$ or a $P2_{1am}(II)$ symmetry, all of which exhibit an electrical polarization and do not require a specific Dy ordering [14]. Which of the proposed symmetries is realized is unknown at present. Standard RSM-mapping is not adequate to provide an answer.

Analogous to bulk, the expectation for the direction of P in orthoferrite thin films is $P||c$, the theoretical prediction for strained orthoferrites is $P||a$ [13, 14]. Practically, [100], [010], [110] and [001] are reported with the emphasis on the latter [49, 50, 53, 54]. For the [001] oriented films, the appearance of an electrical polarization seems to depend on the film composition and antisite or oxygen defects are suggested as the origin [49, 50, 54]. This would be defect-mediated FE [55, 56], potentially slow and requires larger activation barriers for the polarization switching. The polar axis for these films is more likely to be along [001]. However, polarization values reported range between 10.8 and 15.8 μC/cm^2 [49]. For the [010] $YFeO_3$ films polarization values of 15.06 μC/cm^2 at room temperature are reported with $P||b$ [57]. So far, polarization values reported, including 300 K values, are of the order μC/cm^2 and above for orthoferrite thin films. The mechanism responsible for FE can be very different. For the presented (010)-oriented $DyFeO_3$ thin films, a significant contribution to polar properties via defects is excluded since the composition has been regularly checked using Rutherford back scattering, μRaman measurements show no indication of a large number of oxygen vacancies (see S2 [40]).

Measuring a remnant polarization up to 260 K with values larger than 1μC/cm^2 confirms that the theoretical predictions of a ferroelectric phase in orthoferrites near or at room temperature due to lattice strain with large polarization values are realistic [14]. A polar response at 260 K also means that the appearance of polar properties for an orthoferrite thin film has been changed by more than 250 K as compared to bulk. It was typical for films with a thickness larger than 30 nm, that P_{rem} was of the order 0.1 μC/cm^2 or smaller, whereas thinner films approached polarization values of 1 μC/cm^2 or larger even in a temperature range between 200 and 300 K. Which crystalline phase is responsible for the polar phase cannot be verified due to the limited geometry of an epitaxial thin film to fully characterize the structure using X-rays. The high sensitivity of the material to small magnetic fields and probable depolarization effects prevented to directly probe the intrinsic magneto-electric coupling in this magnetically induced ferroelectric material. Where the indicated boundaries in Figure 5 between the amount of compressive strain and a Néel-temperature are, is subject to further work.

3 | Conclusion

In summary, we have studied structural, magnetic and polar properties of compressively strained orthorhombic (010)-oriented $DyFeO_3$ thin films on (010) $YAlO_3$. As a consequence, the inversion symmetry is broken, and the magnetic symmetry is reduced, with both aspects being responsible for the appearance of polar properties. Also, the influence of the Fe-spin lattice

on Dy^{3+} becomes very noticeable, leading to a FM and AFM alignment of the Dy spin relative to the Fe-spin. The growth-induced strain increases T_{SR} by more than 20 K, and unlike for single crystals the transition width is up to 40 K. The change in the spin direction is largely incomplete and blocked, with the consequence that a strained film remains in the Γ_4 phase at all temperatures. For a single crystal, applied fields of up to 100 mT along the *c*-direction reduce T_{SR}, albeit not as strongly as observed for single crystals.

$DyFeO_3$ films demonstrate a polar response up to 260 K with indications of a polar response up to 390 K, moving FE by more than 250 K with respect to bulk. The polar nature of these films is the consequence of breaking the non-polar uc symmetry by lowering the magnetic symmetry due to the strain anisotropy. Unlike in single crystals the polar direction is [100] and not [001]. As a general trend, thinner films show larger polarization values in the $\mu C/cm^2$ range, confirming theoretical predictions of a strain-induced polarization [9]. These findings for $DyFeO_3$ will also apply to most other orthoferrites prepared as strained, coherent thin films.

4 | Experimental Section

4.1 | Sample Fabrication

Epitaxial thin films of $DyFeO_3$ (a = 5.302 Å, b = 5.598 Å and c = 7.623 Å)) and $LuFeO_3$ (a = 5.218 Å, b = 5.556 Å and c = 7.575 Å) are grown on (010) oriented $YAlO_3$ single crystalline substrates (a = 5.180 Å, b = 5.330 Å, and c = 7.375 Å) by pulsed laser deposition using a KrF excimer laser (λ = 248 nm, 3 Hz) with an in-plane lattice mismatch between (010) $DyFeO_3$ and a (010) $YAlO_3$ substrate of -2.36% along the *a*- and -3.36% along the *c*-axis, -5.03% along the *b*-axis [42]. The lattice mismatch for $LuFeO_3$ is -0.73% along the *a*-, -4.23% along *b*-, and -2.71% along the *c*-axis. $YAlO_3$ is a non-magnetic and non-ferroelectric insulating substrate and therefore suitable to study magnetic and dielectric/FE properties of multiferroic films on the same substrate. The laser beam is focused onto a sintered ceramic target with a spot size of 1.4 × 1.4 mm^2 with the laser fluence adjusted to 2.0 Jcm^{-2}. The substrate is located on-axis to the plasma plume with a distance of 5 cm from the target. Deposition was performed in an O_2 background at 0.33 mbar with the substrate heated to 700°C by a lamp heater [42]. Five $DyFeO_3$ films of different thickness have been deposited subsequently (13, 27, 51, 78, 115 nm) to study the thickness dependence of crystalline and magnetic properties. Other films discussed were prepared at different preparation runs with the aforementioned deposition conditions. The composition for the described deposition conditions was verified using Rutherford back scattering. In addition, X-ray absorption measurements showed the correct valence of +3 for the cations and -2 for oxygen. The growth of $LuFeO_3$ was monitored using reflecting high-energy electron diffraction to a thickness of 22 oscillations corresponding to 12.2 nm. For both materials, the composition for the described deposition conditions was verified using Rutherford back scattering. In addition, X-ray absorption measurements showed the correct valence of +3 for the cations, and -2 for oxygen.

4.2 | X-Ray Diffraction

The structural quality and the thickness of the films after the deposition have been monitored by XRD and X-ray reflectometry (XRR), respectively, using a Seifert 3003 PTS and a Bruker D8 Advance four-circle X-ray diffractometers with a Cu $K_{\alpha 1}$ monochromatic X-ray source. Θ-2Θ scans have been used to monitor the crystalline quality of all samples, reciprocal space maps to determine in-plane lattice constants and to evaluate qualitatively strain in these films, and XRR to determine the thickness of the films after the deposition.

4.3 | Magnetic Characterization

The temperature-dependent magnetization was investigated by a commercially available SQUID magnetometer (Quantum Design, MPMS 3). It enables temperature sweeps between 1.8 and 400 K with a magnetic field of up to 7 T parallel to the measurement direction. The zero-field cooled (ZFC) measurements of the magnetic moment (M) along [100], [010] and [001] have been conducted with probing fields between 10 and 100 mT.

4.4 | Raman Spectroscopy

Raman spectra were obtained using a *LabRAM Series* Raman Microscope (*Horiba Jobin Yvon*) equipped with a He–Ne excitation laser (λ: 632.8 nm, output power: ∼ 20 mW) by focusing on the film surface with a 100x objective. The $DyFeO_3$ single crystal and (010)-oriented $DyFeO_3$ film have been aligned with respect to the laser polar axis to measure the Raman signal with respect to the crystalline axis. As a reference for the $DyFeO_3$ film grown on $YAlO_3$, a bare (010)-oriented $YAlO_3$ single crystal substrate has been measured following the same procedure. The signals shown are as measured. To remove the background, the software options of the Jobin-Yvon Raman package LabRam 5 have been used. To verify the consistency of the Raman spectra, we used single crystal Si as a reference.

4.5 | Optical SHG

SHG is a nonlinear optical process denoting the emission of light at frequency 2ω from a crystal irradiated with light at frequency ω. This is expressed by the equation $P_i(2\omega) = \varepsilon_0 \Sigma_{j,k} \chi^{(2)}_{ijk} E_j(\omega) E_k(\omega)$, where $E_{j,k}(\omega)$ and $P_i(2\omega)$ are the electric-field components of the incident light and of the nonlinear polarization, respectively, with the latter acting as the source of the SHG wave. The nonlinear susceptibility $\chi^{(2)}_{ijk}$ characterizes the ferroelectric state.

At room temperature single crystal AFM $RFeO_3$ possesses the magnetic point group symmetry m'm'2 and has no net polarization [4]. Any symmetry breaking would reduce this symmetry, thereby introducing a polar component. To probe polar properties of strained (010) oriented $DyFeO_3$ and $LuFeO_3$, we used a refecltion geometry and a 1 kHz amplified Ti:sapphire laser system with an optical parametric amplifier. The light pulses

with a wavelength of 1200 nm had a pulse length of 60 fs and a pulse energy of 25 μJ. Detailed technical aspects of SHG in ferroic systems and especially in $DyFeO_3$ are described in Refs. [58–60]. As a reference a $BaTiO_3$ film is used.

4.6 | Ferroelectric Measurements

To evaluate in-plane electric properties of films, Au (56 nm)/Ti (4 nm) interdigitated electrodes were patterned on the film surface by photolithography and lift-off procedures. The finger width and gap are 5 μm, and the line length is 1.25 mm. The maximum number of fingers patterned was 361. Measurements were performed in helium and the temperature was controlled by a LakeShore Model 325 temperature controller. Capacitance measurements were performed using an Agilent E4980A LCR meter at zero DC field with an AC voltage of 100 mV. The frequency was varied from 100 to 2 MHz. The FE hysteresis curve ($P(E)$-loop) was probed with the Positive-Up Negative-Down (PUND, double-wave) protocol [61] using National Instruments compact DAQ analogue input (NI 9229)/output (NI 9263) modules and a home-made Sawyer-Tower circuit with a drive voltage of 50 V and drive frequency of 250 Hz. The polarization (P) was calculated as $P = Q(tL)^{-1}$ [62, 63], where Q is the measured charge, t is the film thickness, and L is the total length of the finger pairs.

Acknowledgements

This work was supported by the Swiss National Science Foundation (Project Nos. 200020_169393 and 200021_236413) and the Paul Scherrer Institute. M.T. and B.Y. acknowledged the ETH Zurich Research Grant funding under reference 22-2 ETH-016.

Open access publishing facilitated by ETH-Bereich Forschungsanstalten, as part of the Wiley - ETH-Bereich Forschungsanstalten agreement via the Consortium Of Swiss Academic Libraries.

Conflicts of Interest

The authors declare no conflicts of interest.

Data Availability Statement

The data that support the findings of this article are available upon reasonable request.

References

1. R. L. White, "Review of Recent Work on the Magnetic and Spectroscopic Properties of the Rare-Earth Orthoferrites," *Journal of Applied Physics* 40 (1969): 1061–1069, https://doi.org/10.1063/1.1657530.

2. D. Treves, "Magnetic Studies of Some Orthoferrites," *Physical Review* 125 (1962): 1843–1853, https://doi.org/10.1103/PhysRev.125.1843.

3. S. J. Yuan, W. Ren, F. Hong, et al., "Spin Switching and Magnetization Reversal in Single-Crystal $NdFeO_3$," *Physical Review B* 87 (2013): 184405, https://doi.org/10.1103/PhysRevB.87.184405.

4. Y. Tokunaga, S. Iguchi, T. Arima, and Y. Tokura, "Magnetic-Field-Induced Ferroelectric State in $DyFeO_3$," *Physical Review Letters* 101 (2008): 097205.

5. J. Wang, J. Liu, J. Sheng, et al., "Simultaneous Occurrence of Multiferroism and Short-Range Magnetic Order in $DyFeO_3$," *Physical Review B* 93 (2016): 140403, https://doi.org/10.1103/PhysRevB.93.140403.

6. Z. Y. Zhao, X. Zhao, H. D. Zhou, et al., "Ground State and Magnetic Phase Transitions of Orthoferrite $DyFeO_3$," *Physical Review B* 89 (2014): 224405.

7. A. Stroppa, M. Marsman, G. Kresse, and S. Picozzi, "The Multiferroic Phase of $DyFeO_3$: An Ab Initio Study," *New Journal of Physics* 12 (2010): 093026, https://doi.org/10.1088/1367-2630/12/9/093026.

8. B. Rajeswaran, D. Sanyal, M. Chakrabarti, Y. Sundarayya, A. Sundaresan, and C. N. R. Rao, "Interplay of 4f-3d Magnetism and Ferroelectricity in $DyFeO_3$," *EPL* 101 (2013): 17001.

9. J.-H. Lee, Y. K. Jeong, J. H. Park, et al., "Spin-Canting-Induced Improper Ferroelectricity and Spontaneous Magnetization Reversal in $SmFeO_3$," *Physical Review Letters* 107 (2011): 117201, https://doi.org/10.1103/PhysRevLett.107.117201.

10. Z. Y. Zhao, X. M. Wang, C. Fan, et al., "Magnetic Phase Transitions and Magnetoelectric Coupling of $GdFeO_3$ Single Crystals Probed by Low-Temperature Heat Transport," *Physical Review B* 83 (2011): 014414, https://doi.org/10.1103/PhysRevB.83.014414.

11. E. Bousquet and A. Cano, "Non-Collinear Magnetism in Multiferroic Perovskites," *Journal of Physics: Condensed Matter* 28 (2016): 123001, https://doi.org/10.1088/0953-8984/28/12/123001.

12. S. Cao, L. Chen, W. Zhao, et al., "Tuning the Weak Ferromagnetic States in Dysprosium Orthoferrite," *Scientific Reports* 6 (2016): 37529, https://doi.org/10.1038/srep37529.

13. H. J. Zhao, W. Ren, Y. Yang, X. M. Chen, and L. Bellaiche, "Effect of Chemical and Hydrostatic Pressures on Structural and Magnetic Properties of Rare-Earth Orthoferrites: A First-Principles Study," *Journal of Physics: Condensed Matter* 25 (2013): 466002, https://doi.org/10.1088/0953-8984/25/46/466002.

14. Z. Hong Jian, Y. Yurong, R. Wei, M. Ai-Jie, C. Xiang Ming, and B. Laurent, "Creating Multiferroics With Large Tunable Electrical Polarization From Paraelectric Rare-Earth Orthoferrites," *Journal of Physics: Condensed Matter* 26 (2014): 472201.

15. S. Tamulevičius, "Stress and Strain in the Vacuum Deposited Thin Films," *Vacuum* 51 (1998): 127–139, https://doi.org/10.1016/S0042-207X(98)00145–6.

16. G. Abadias, E. Chason, J. Keckes, et al., "Review Article: Stress in Thin Films and Coatings: Current Status, Challenges, and Prospects," *Journal of Vacuum Science & Technology A* 36 (2018): 020801, https://doi.org/10.1116/1.5011790.

17. M. Behrens, A. Lotnyk, J. W. Gerlach, and B. Rauschenbach, "Strain-Induced Phase Selection in Epitaxial $Ge_2Sb_2Te_5$ Thin Films," *Physical Review Materials* 4 (2020): 015001, https://doi.org/10.1103/PhysRevMaterials.4.015001.

18. B. Abhijit and J. Yoon Hee, *Epitaxy*, ed. Z. Mia. (IntechOpen, 2017).

19. T. Tiittanen and M. Karppinen, "Structure Evolution Upon Chemical and Physical Pressure in $(Sr_{1-x}Ba_x)_2FeSbO_6$," *Journal of Solid State Chemistry* 246 (2017): 245–251, https://doi.org/10.1016/j.jssc.2016.11.033.

20. R. S. Liu, C. H. Shen, S. F. Hu, and J. M. Chen, "Chemical Pressure Control of Curie Temperature in $La_{0.6}(Ba_{0.4-x}Ca_x)MnO_3$," *Materials Chemistry and Physics* 75 (2002): 26–31, https://doi.org/10.1016/S0254-0584(02)00025-1.

21. F. Mumtaz, S. Nasir, G. H. Jaffari, and S. I. Shah, "Chemical Pressure Exerted by Rare Earth Substitution in $BiFeO_3$: Effect on Crystal Symmetry, Band Structure and Magnetism," *Journal of Alloys and Compounds* 876 (2021): 160178, https://doi.org/10.1016/j.jallcom.2021.160178.

22. D. G. Schlom, L.-Q. Chen, C. J. Fennie, et al., "Elastic Strain Engineering of Ferroic Oxides," *MRS Bulletin* 39 (2014): 118–130, https://doi.org/10.1557/mrs.2014.1.

23. K. J. Choi, M. Biegalski, Y. L. Li, et al., "Enhancement of Ferroelectricity in Strained $BaTiO_3$ Thin Films," *Science* 306 (2004): 1005–1009, https://doi.org/10.1126/science.1103218.

24. J. H. Haeni, P. Irvin, W. Chang, et al., "Room-Temperature Ferroelectricity in Strained $SrTiO_3$," *Nature* 430 (2004): 758–761, https://doi.org/10.1038/nature02773.

25. D. Sando, "Strain and Orientation Engineering in ABO_3 Perovskite Oxide Thin Films," *Journal of Physics: Condensed Matter* 34 (2022): 153001, https://doi.org/10.1088/1361-648X/ac4c61.

26. P. E. Janolin, A. S. Anokhin, Z. Gui, et al., "Strain Engineering of Perovskite Thin Films Using a Single Substrat," *Journal of Physics: Condensed Matter* 26 (2014): 292201, https://doi.org/10.1088/0953-8984/26/29/292201.

27. S. Dhole, A. Chen, W. Nie, B. Park, and Q. Jia, "Strain Engineering: A Pathway for Tunable Functionalities of Perovskite Metal Oxide Films," *Nanomaterials* 12 (2022): 835.

28. F. K. Chiang, M. W. Chu, F. C. Chou, et al., "Effect of Jahn-Teller Distortion on Magnetic Ordering in $Dy(Fe,Mn)O_3$ Perovskites," *Physical Review B* 83 (2011): 245105, https://doi.org/10.1103/PhysRevB.83.245105.

29. E. F. Bertaut, J. Chappert, J. Mareschal, J. P. Rebouillat, and J. Sivardière, "Structures Magnetiques de $TbFeO_3$," *Solid State Communications* 5 (1967): 293–298, https://doi.org/10.1016/0038-1098(67)90276-1.

30. Y.-J. Ke, X.-Q. Zhang, H. Ge, Y. Ma, and Z.-H. Cheng, "Low Field Induced Giant Anisotropic Magnetocaloric Effect in $DyFeO_3$ Single Crystal," *Chinese Physics B* 24 (2015): 037501, https://doi.org/10.1088/1674-1056/24/3/037501.

31. B. Biswas, V. F. Michel, Ø. S. Fjellvåg, et al., "Role of Dy on the Magnetic Properties of Orthorhombic $DyFeO_3$," *Physical Review Materials* 6 (2022): 074401, https://doi.org/10.1103/PhysRevMaterials.6.074401.

32. C. Ritter, R. Vilarinho, J. A. Moreira, M. Mihalik, M. Mihalik, and S. Savvin, "The Magnetic Structure of $DyFeO_3$ Revisited: Fe Spin Reorientation and Dy Incommensurate Magnetic Order," *Journal of Physics: Condensed Matter* 34 (2022): 265801, https://doi.org/10.1088/1361-648X/ac6787.

33. S. E. Nikitin, N. D. Andriushin, Ø. S. Fjellvåg, et al., "Competition Between Multiferroic and Magnetic Soliton Lattice States in $DyFeO_3$," *Physical Review Research* 7 (2025): 043173, https://doi.org/10.1103/kwrl-x4hw.

34. T. Nakajima, Y. Tokunaga, Y. Taguchi, Y. Tokura, and T.-H. Arima, "Piezomagnetoelectric Effect of Spin Origin in Dysprosium Orthoferrite," *Physical Review Letters* 115 (2015): 197205, https://doi.org/10.1103/PhysRevLett.115.197205.

35. R. Saha, A. Sundaresan, and C. N. R. Rao, "Novel Features of Multiferroic and Magnetoelectric Ferrites and Chromites Exhibiting Magnetically Driven Ferroelectricity," *Materials Horizons* 1 (2014): 20–31, https://doi.org/10.1039/C3MH00073G.

36. A. Sasani, J. Íñiguez, and E. Bousquet, "Origin of Nonlinear Magnetoelectric Response in Rare-Earth Orthoferrite Perovskite Oxides," *Physical Review B* 105 (2022): 064414, https://doi.org/10.1103/PhysRevB.105.064414.

37. T. Yamaguchi and K. Tsushima, "Magnetic Symmetry of Rare-Earth Orthochromites and Orthoferrites," *Physical Review B* 8 (1973): 5187–5198, https://doi.org/10.1103/PhysRevB.8.5187.

38. B. Biswas, P. Naumov, F. Motti, et al., "Correlation of Structural and Magnetic Properties of $RFeO_3$ (R=Dy,Lu)," *Physical Review Materials* 8 (2024): 084404, https://doi.org/10.1103/PhysRevMaterials.8.084404.

39. M. C. Weber, M. Guennou, H. J. Zhao, et al., "Raman Spectroscopy of Rare-Earth Orthoferrites $RFeO_3$ (R =La, Sm, Eu, Gd, Tb, Dy)," *Physical Review B* 94 (2016): 214103, https://doi.org/10.1103/PhysRevB.94.214103.

40. *See Supplemental Material [link to be inserted by publisher].*

41. B. Biswas, F. Stramaglia, E. V. Pomjakushina, T. Lippert, C. A. F. Vaz, and C. W. Schneider, "Room Temperature Dy Spin-Flop Switching in Strained $DyFeO_3$ Thin Films," *Advanced Materials Interfaces* 12 (2025): 2400938, https://doi.org/10.1002/admi.202400938.

42. B. Biswas, *Strain-Induced Magnetoelectric Properties of Epitaxial (010) o-$DyFeO_3$ (Thin Films PhD thesis, ETH Zurich*, 2021).

43. C. M. Hurd, "Varieties of Magnetic Order in Solids," *Contemporary Physics* 23 (1982): 469–493, https://doi.org/10.1080/00107518208237096.

44. M. V. Medvedev and S. M. Goryainova, "Asperomagnetism and Short-Range Magnetic Order in a Heisenberg Magnet With Random Exchange Bonds of Different Signs," *Physica Status Solidi (b)* 98 (1980): 143–154, https://doi.org/10.1002/pssb.2220980114.

45. M. Fiebig, "Covering the Fruitful Combination of Nonlinear Optics and Ferroic Materials," *Nonlinear Optics on Ferroic Materials* (Wiley-VCH, 2023): 31–89, https://doi.org/10.1002/9783527822812.

46. K. Shimamoto, Y. W. Windsor, Y. Hu, et al., "Multiferroic Properties of Uniaxially Compressed Orthorhombic $HoMnO_3$ Thin Films," *Applied Physics Letters* 108 (2016): 112904, https://doi.org/10.1063/1.4944460.

47. K. Shimamoto, S. Mukherjee, S. Manz, et al., "Tuning the Multiferroic Mechanisms of $TbMnO_3$ by Epitaxial Strain," *Scientific Reports* 7 (2017): 44753, https://doi.org/10.1038/srep44753.

48. S. Mukherjee, K. Shimamoto, C. W. Schneider, and C. Niedermayer, "Unique Coexistence of Incommensurate and Commensurate Magnetic Order in $TbMnO_3$ Strained Films," *Physical Review Materials* 3 (2019): 104412, https://doi.org/10.1103/PhysRevMaterials.3.104412.

49. S. Ning, A. Kumar, K. Klyukin, et al., "An Antisite Defect Mechanism for Room Temperature Ferroelectricity in Orthoferrites," *Nature Communications* 12 (2021): 4298, https://doi.org/10.1038/s41467-021-24592-w.

50. E. Cho, K. Klyukin, T. Su, A. Kaczmarek, and C. A. Ross, "Composition-Dependent Ferroelectricity of $LuFeO_3$ Orthoferrite Thin Films," *Advanced Electronic Materials* 9 (2023): 2300059, https://doi.org/10.1002/aelm.202300059.

51. T. N. Stanislavchuk, Y. Wang, Y. Janssen, G. L. Carr, S. W. Cheong, and A. A. Sirenko, "Magnon and Electromagnon Excitations in Multiferroic $DyFeO_3$," *Physical Review B* 93 (2016): 094403, https://doi.org/10.1103/PhysRevB.93.094403.

52. S. Rajput, P. Balasubramanian, A. Singh, et al., "Coexisting Magnetic Structures and Spin Reorientation in $Er_{0.5}Dy_{0.5}FeO_3$: Bulk Magnetization, Neutron Scattering, Specific Heat, and Density Functional Theory Studies," *Physical Review B* 105 (2022): 214436, https://doi.org/10.1103/PhysRevB.105.214436.

53. W. Si, K. Huang, X. Wu, and S. Feng, "Epitaxial Thin Film of $SmFeO_3$ Ferroelectric Heterostructures," *Science China Chemistry* 57 (2014): 803–806, https://doi.org/10.1007/s11426-014-5099-6.

54. H. Li, Y. Yang, S. Deng, et al., "Role of Oxygen Vacancies in Colossal Polarization in $SmFeO_{3-\delta}$ Thin Films," *Science Advances* 8, no. 13 (2022): abm8550, https://doi.org/10.1126/sciadv.abm8550.

55. C. Ricca and U. Aschauer, "Mechanisms for Point Defect-Induced Functionality in Complex Perovskite Oxides," *Applied Physics A* 128 (2022): 1083, https://doi.org/10.1007/s00339-022-06210-8.

56. K. Klyukin and V. Alexandrov, "Effect of Intrinsic Point Defects on Ferroelectric Polarization Behavior of $SrTiO_3$," *Physical Review B* 95 (2017): 035301, https://doi.org/10.1103/PhysRevB.95.035301.

57. M. Shang, C. Wang, Y. Chen, F. Sun, and H. Yuan, "The Multiferroic Epitaxial Thin Film $YFeO_3$," *Materials Letters* 175 (2016): 23–26, https://doi.org/10.1016/j.matlet.2016.03.047.

58. M. Fiebig, V. V. Pavlov, and R. V. Pisarev, "Second-Harmonic Generation as a Tool for Studying Electronic and Magnetic Structures of Crystals: Review," *Journal of the Optical Society of America B* 22 (2005): 96–118, https://doi.org/10.1364/JOSAB.22.000096.

59. M. Matsubara, S. Manz, M. Mochizuki, et al., "Magnetoelectric Domain Control in Multiferroic $TbMnO_3$," *Science* 348 (2015): 1112–1115.

60. E. Hassanpour, Y. Zemp, Y. Tokunaga, et al., "Magnetoelectric Transfer of a Domain Pattern," *Science* 377 (2022): 1109–1112, https://doi.org/10.1126/science.abm3058.

61. M. Fukunaga and Y. Noda, "New Technique for Measuring Ferroelectric and Antiferroelectric Hysteresis Loops," *Journal of the Physical Society of Japan* 77 (2008): 064706–064706, https://doi.org/10.1143/JPSJ.77.064706.

62. B. Xu, R. G. Polcawich, S. Trolier-McKinstry, et al., "Sensing Characteristics of In-Plane Polarized Lead Zirconate Titanate Thin Films," *Applied Physics Letters* 75 (1999): 4180–4182, https://doi.org/10.1063/1.125575.

63. Q. Q. Zhang, S. J. Gross, S. Tadigadapa, T. N. Jackson, F. T. Djuth, and S. Trolier-McKinstry, "Lead Zirconate Titanate Films for d_{33} Mode Cantilever Actuators," *Sensors and Actuators A: Physical* 105 (2003): 91–97, https://doi.org/10.1016/S0924-4247(03)00068-2.

Supporting Information

Additional supporting information can be found online in the Supporting Information section.

Supporting File: aelm70533-sup-0001-SuppMat.docx.